Late Quaternary sea level changes of the Persian Gulf

Stephen W. Lokier [a,*], Mark D. Bateman [b], Nigel R. Larkin [c], Philip Rye [d] and John R. Stewart [e]

[a] Petroleum Geosciences Department, The Petroleum Institute, P.O. Box 2533, Abu Dhabi, United Arab Emirates (slokier@pi.ac.ae)

[b] Department of Geography, Winter St., University of Sheffield, Sheffield, S10 2TN, UK (M.D.Bateman@sheffield.ac.uk)

[c] Cambridge University Museum of Zoology, Downing Street, Cambridge, CB2 3EJ, UK (nrlarkin@easynet.co.uk)

[d] Granary Court Cottage, Granary Court Road, Smeeth, Ashford, Kent, TN25 6RE, UK (phil_rye@hotmail.com)

[e] School of Science and Technology, Bournemouth University Talbot Campus, Fern Barrow Poole, Dorset, BH12 5BB, UK (jstewart@bournemouth.ac.uk)

[*] Corresponding author.

E-mail address: slokier@pi.ac.ae (S. Lokier)

Abstract

Late Quaternary reflooding of the Persian Gulf climaxed with the mid-Holocene highstand previously variously dated between 6 – 3.4 ka. Examination of the stratigraphic and palaeoenvironmental context of a mid-Holocene whale beaching allows us to accurately constrain the timing of the transgressive, highstand and regressive phases of the mid- to late Holocene sea level highstand in the Persian Gulf. Mid-Holocene transgression of the Gulf surpassed today's sea level by 7100-6890 cal yr BP, attaining a highstand of > 1 m above current seal level shortly after 5290-4570 cal yr BP before falling back to current levels by 1440-1170 cal yr BP. The cetacean beached into an intertidal hardground pond during the transgressive phase (5300-4960 cal yr BP) with continued transgression interring the skeleton in shallow-subtidal sediments. Subsequent relative sea level fall produced a forced regression with consequent progradation of the coastal system. These new dates refine previously reported timings for the mid- to late Holocene sea level highstand published for other regions. By so doing, they allow us to more accurately constrain the timing of this correlatable global eustatic event.

Keywords: Persian Gulf; Arabian Gulf; Sabkha; Sea level; OSL; Quaternary

Introduction

The present-day morphology of the Abu Dhabi coastline of the United Arab Emirates is interpreted to have developed during the late Holocene as sediment accreted around Pleistocene age limestone cores, associated with the eastern termination of the Great Pearl Bank, and prograded into the recently-flooded Persian Gulf (e.g. Evans et al., 1969; Lokier and Steuber, 2008; Purser and Evans, 1973). However, establishing the timing of the Holocene sea level maximum for the Persian Gulf, and, hence, the initiation of late Holocene progradation of the Abu Dhabi shoreline, has been problematical. This study employs sedimentary sections hosting a cetacean skeleton as a data source to provide new evidence for the constraint of the Holocene sea level maximum in the Persian Gulf.

During the Last Glacial Maximum (LGM), between 26.5 and 19 ka (Clark et al., 2009), eustatic sea level lay between 120 – 130 m lower than present-day sea level (Clark et al., 2009; Fleming et al., 1998; Hanebuth et al., 2009; Peltier and Fairbanks, 2006). During this time, the sea floor of the Persian Gulf was exposed and terrestrial aeolian processes became dominant. The northwesterly Shamal wind blew sand, sourced from Iran, towards the south and east and an extensive dune system developed over much of the basin floor (Sarnthein, 1972). With the end of the LGM, between 20-19 ka (Clark et al., 2009; Yokoyama et al., 2000), a pulse of fresh water caused a rapid sea level rise of 10 m (Clark et al., 2009; Hanebuth et al., 2009), followed by a slower, relatively sedate, increase. Marine waters reached the Strait of Hormuz at approximately 14 ka and by 12.5 ka had entered the Gulf itself and a true seaway had been established (Lambeck, 1996).

The objectives of this study are to utilise a whale beaching event to refine the timing and amplitude of the Holocene sea level maximum in the Persian Gulf and establish the palaeoenvironmental and sequence stratigraphic context of the coastal system at that time. By understanding these factors it will be possible to establish better-constrained sedimentological and stratigraphic models for the development of the Holocene sabkhas of the southern shoreline of the Persian Gulf. These systems are the oft-cited analogue for many of the petroleum reservoirs of the Middle East, thus, an understanding of their mode of formation is imperative to the interpretation of ancient petroleum systems and the development of accurate reservoir models.

Location of study area

The study site lies in the Mussafah Channel situated in the Mussafah Industrial Zone of Abu Dhabi (Fig. 1). The Mussafah Channel is an 8.3 km long dredged channel that was excavated through the coastal Sabkha sequence during the early 1980's. As no further development of the channel took place, the unsupported walls collapsed and eroded back to expose fresh surfaces. Erosion continued until 2006 when a cetacean mandible was exposed at the eastern termination of the channel. Excavation revealed a largely-intact skeleton of a baleen whale of the genus *Megaptera* (Stewart et al., 2011) of which the front 10 m was recovered, including the most-diagnostic cranial and forelimb parts.

Geographic and climatic setting

The Persian Gulf is a shallow epicontinental sea lying in a crescentic northwest to southeast oriented basin floored by the continental crust of the northern margin of the Arabian Plate (Fig. 1). The Zagros Mountains bound the northern shores while the south and west shorelines are bordered by the low-relief Arabian Peninsula. Water depths are shallow, with an average depth of 35 m and rarely exceed 100 m. The floor of the Gulf dips gently north-eastward with the deepest water areas lying close to the southern coast of Iran.

The Persian Gulf coastline of the emirate of Abu Dhabi forms part of a low-angle carbonate ramp depositional system. The supratidal zone of this ramp is characterised by an active sabkha setting in which Recent evaporite minerals are precipitating within the shallow subsurface and an ephemeral halite crust at the surface (Lokier, 2012). The sabkha grades seawards into a broad intertidal mud flat with well-developed microbial mat communities characterising the upper intertidal zone and a polygonal hardground in the lower intertidal zone (Lokier and Steuber, 2009). The hardground extends offshore into the shallow, carbonate-dominated subtidal setting. The mainland coast of Abu Dhabi is locally protected from open-marine conditions by a number of peninsulas and offshore shoals and islands (Fig. 1) associated with the east–west trending Great Pearl Bank. The limited fetch of the Persian Gulf inhibits wave development, thus, low-energy conditions dominate. The tidal regime of the Persian Gulf is microtidal (1–2 m).

The very low-angle geometry of the Abu Dhabi coastline results in this region being extremely sensitive to fluctuations in sea level. Even small changes in relative sea level will result in significant lateral shifts in facies belts. For example, current estimates of eustatic sea level rise of 3.3 mm/yr (Cazenave and Nerem, 2004; Leuliette et al., 2004) would result in marine transgression of the Abu Dhabi shoreline at a rate of 8.25 m/yr. This transgression is, to some extent, countered by progradation of the sabkha system (Lokier and Steuber, 2008). The sensitivity of this coastal system to minor sea level fluctuations provides an opportunity to apply these findings beyond the immediate region of the Persian Gulf to further constrain the timing and extent of the mid- to late Holocene global sea level highstand.

The climate at the Abu Dhabi coast is extremely arid with a mean annual precipitation of 72 mm (Raafat, 2007). Rainfall is often extremely localised, occurring as brief heavy rainstorms concentrated during the months of February and March. Some regions may not experience any rainfall for periods in excess of a year. Evaporation rates are high with an annual mean of 2.75 m (Bottomley, 1996) resulting in elevated salinities of 45–46 g l^{-1} along the open-marine coast of Abu Dhabi and up to 89 g l^{-1} in restricted lagoons (Lokier and Steuber, 2009). Coastline temperatures 50 km west of Abu Dhabi City range between 7°C at night during the winter and 50°C during daytime in the summer (Lokier et al., 2013). The prevailing wind is the north-westerly Shamal. The shallow warm waters of the coast generate high coastal humidity, often reaching 100% during summer months.

Methodology

The site was surveyed utilising a Leica total station employing the Admiralty Chart Datum of mean lowest calculated astronomical tide. The stratigraphy of the sediments was recorded in detail at three locations, facies geometries were characterised and representative sediment samples were collected throughout the profile. Unconsolidated sediment samples were prepared as twenty four resin-impregnated thin sections. Thin sections were subjected to modal analysis, 200 points, in order to quantify the proportions of component allochems. In order to further characterise sedimentary facies, thin sections were examined using standard light microscopy on a polarising microscope. Sediment and skeletal allochem samples were also collected from throughout the excavation site with particular attention being given to their relationship to the cetacean bones.

Five samples were designated for radiocarbon analysis via accelerator mass spectrometry (AMS) at the ^{14}Chrono Centre, Queens University, Belfast. During sample selection, skeletal material from deposit-feeding organisms was avoided as these organisms may ingest detrital ancient carbon which will become incorporated into their shells and significantly offset ^{14}C ages. All of the selected samples were subjected to detailed examination in order to protect against taphonomic processes that would bias radiocarbon analysis. The selected material comprised three bivalves, one barnacle and one specimen of cetacean bone. Unfortunately, the initial elemental analysis of the sample of whale bone (MUS 17B) indicated that there was insufficient remaining protein to undertake radiocarbon dating. All of the ^{14}C results are presented as conventional radiocarbon ages employing the Libby half-life method (Stuiver and Polach, 1977). Results were calibrated using the CALIB (version 7.0.0) calibration program (Stuiver and Reimer, 1993) employing a marine calibration curve and a regional reservoir age correction (ΔR) of 180 ± 53 (Hughen et al., 2004).

Optically stimulated luminescence (OSL) dating was undertaken on three samples collected from sediment found directly adjacent to the whale skeleton. Samples were analysed at the Luminescence Dating Laboratory of the Sheffield Centre for Drylands Research (SCIDR). The palaeodose of quartz grains was measured on 9.6 mm diameter aliquots by employing a modified form of the single aliquot regenerative (SAR) method (Murray and Wintle, 2000) using a Risø TL DA-20 luminesce reader with radiation doses administered from a calibrated ^{90}strontium beta source. An experimentally derived preheat of 180°C for 10 seconds and a cut-heat of 160°C was used within the SAR. During testing with infrared stimulated luminescence (IRSL) it was found that a residual feldspar signal existed within the samples (possibly due to feldspars included within quartz), which was removed prior to each OSL SAR measurement with an IRSL wash for 40 seconds at 50°C (Banerjee et al., 2001; Wilson et al., 2008). Reproducibility was established by undertaking up to 24 replicate palaeodoses on each sample. The above methodology was validated with a dose recovery test on sample Shfd11039 which returned a given to recovered dose ratio of 0.97 ± 0.02. Final palaeodoses for each samples were derived from this replicate data using the central age model (Galbraith and Green, 1990) excluding outliers (those aliquots outside 2 standard deviations of the mean). Elemental concentrations were determined from ICP-MS analysis with the resultant uranium, thorium, rubidium and potassium values being used, once suitably attenuated for moisture (a saturation value of 30 ± 5% was applied), size and density to calculate sample dose rates. Cosmogenic contributions were calculated using the algorithm of Prescott and Hutton (1994).

Samples for the analysis of $\delta^{18}O$ and $\delta^{13}C$ were prepared from three thick sections of articulated filter-feeding bivalves. Powder was milled from the thick sections parallel to growth bands using a 0.8 mm diameter tungsten drill bit. Samples were analysed at GeoZentrum Nordbayern using a Gasbench II connected to a ThermoFinnigan Five Plus mass spectrometer. External reproducibility is better than 0.1‰ $\delta^{18}O$ and $\delta^{13}C$ at 2 sigma.

Results

Stratigraphic context of the cetacean skeleton

Three stratigraphic sections were logged in detail for this study (Fig. 2). The sections all lie on a north-south transect along the eastern wall of the Mussafah Channel, and were selected in order to avoid areas with any evidence of anthropogenic disturbance. The central section (MC-3) lies within the excavation site and records the relationship between sedimentary facies and the skeleton (Figs 3 & 4).

The base of the stratigraphic succession is only observed in section MC-1 where it comprises a grey peloidal and bioclastic carbonate sand with large gypsum lathes up to 30 cm in diameter (Table 1, Figs 2 & 5). This horizon is overlain by a locally-degraded laminated microbial mat containing isolated bioclasts bound within the laminations. The microbial mat horizon is overlain by a carbonate-cemented planar hardground dominated by bioclasts but with isolated gypsum lathes. The planar surface of the hardground lacks any evidence of encrustation or boring. Above the hardground, locally-laminated peloidal bioclastic carbonate sand becomes increasingly mud-dominated up-section (Table 1) before passing into a horizon of bioturbated, poorly-laminated muddy facies that again contains peloids and bioclasts. This horizon is locally bioturbated by mm-wide sub-vertical burrows with distinctive dark-brown margins. Locally cross-bedded bioclastic gravels, dominated by gastropods, bivalves and peneroplid foraminifera, are banked against some of the bones of the skeleton, these gravel banks do not exhibit any preferred orientation. The succeeding unit is a peloid and bioclastic sand with mud. The top of the succession comprises gypsum gravel with an increasing anhydrite component in the uppermost portion (Table 1). The anhydrite is locally distorted to form an enterolithic texture (Figs 2 & 4B). Gypsum lathes occur throughout the succession with a decrease in size up-section. Siliciclastic material was only observed in the hardground and underlying units (Fig. 5). A series of iron-oxide stained horizons occur at a depth of 26-53 cm below the surface of the sediment; these stains form bands between 1-4 cm in thickness with the most-stained and thickest band occurring at their base (Figs 2 & 4B).

The skeleton of the cetacean lies, in an inverted position, atop the hardground within the peloidal bioclastic carbonate sand and mud horizons. The lower portions of the jaws and skull locally penetrate into, and are embedded within, the underlying hardground. Locally, articulated bivalves (*Saccostrea*) were found attached to the ribs close to the vertebrae. The sediments adjacent to the skeleton exhibit lateral variability both in terms of grain size and component allochems (Table 1).

Dating the stratigraphic sequence

The calculated radiocarbon dates are presented in Table 2 along with the calibrated age ranges and delta ^{13}C values for the samples. The reported $\delta^{13}C$ values are appropriate for the nature of the materials being considered in the study (Walker, 2005). The calibrated ages are internally consistent with the oldest date (6887-6567 cal yr BP) being recorded from the hardground, an age of 5304-4957 cal yr BP being recorded for a barnacle identified as *Coronula diadema* that is believed to have been attached to the whale's skin in life (Stewart et al., 2011) and so dates the whale at death and the youngest ages (5285-4574 cal yr BP) being recorded from the sediments surrounding the skeleton. These dates are consistent with previously published radiocarbon dates for the upper part of the Mussafah Channel sedimentary sequence (Stewart et al., 2011; Strohmenger et al., 2010). Previously reported ages for the microbial mat range between 6230-7103 cal yr BP (Stewart et al., 2011) but must predate the hardground that has been dated at 6887-6567 cal yr BP. Thus, we can constrain the age of the microbial mat to between 7103-6887 cal yr BP.

The results of the OSL analysis are presented in Table 3 along with palaeodose and calculated dose rates for the samples. The derived ages, of between 3.18 ± 0.24 – 2.51 ka ± 0.14, are also internally consistent but are significantly younger than those calculated for the equivalent horizons using radiocarbon analysis. These large discrepancies between the radiocarbon dates and the dates derived from OSL are a cause for concern. As stated, the radiocarbon dates are consistent with ages published from earlier studies of the Abu Dhabi Sabkha sequence, it is therefore inferred that the OSL dates are problematical.

The OSL replicate palaeodose data is essentially normally distributed, showing little scatter apart from an occasional outlier (2, 4 and 5 aliquots from Shfd11039-42 respectively) and a dose can be recovered successfully in the lab. It would appear unlikely that the OSL ages are too young as a result of mixing in of younger sediment due to bioturbation (Bateman et al., 2007) or incorrect measurement.

OSL relies on establishing the average burial environmental dose rate in order to calculate the age of the sample. Environmental dose rate is controlled by the presence of radioactive elements (uranium (U), thorium (Th) , rubidium (Rb), potassium-40 (K)) and cosmic rays. The presence of water is also important as it absorbs radiation differently from the sediment (Lian et al., 1995). During OSL date calculation, it was assumed that the average moisture since burial was at saturation (30%). This assumption is based on the presence of the iron-stained horizons which show that, prior to the excavation of the Mussafah Channel, the site lay wholly below the water table. This then is not the source of OSL age under-estimation.

Both uranium and potassium are soluble, therefore it is possible that fluctuating saline groundwater, coupled with a high evaporation rate, could have modified the environmental radiation dose since burial by leaching and concentrating these elements. Whilst it is not possible to reconstruct changes of dose rate through time, two observations can be made. Firstly, both U and K increase with depth and secondly the Th:U ratio for the three samples is 0.22, this is significantly different than the upper continental crustal average (UCC) of 3.82 (Taylor and McClennan, 1985). It is therefore possible that the elemental concentrations, as measured, do not reflect the average concentrations during the burial history of the sediments. Similar disequilibrium issues were identified in Wood et al. (2012) and Stevens et al. (2014) from Persian coastal samples. In these studies, conservative (large) uncertainties were applied to correct ages for disequilibrium. In the current study we can show with the benefit of the independent radiocarbon chronology that this approach doesn't work for young samples. If, however, an average UCC is applied to the data by reducing the U concentrations (i.e. assuming present-day values reflect recent concentration) OSL ages are brought into line with those of radiocarbon (5.31 ±0.27 to 6.76 ±0.34 ka; Table 3). The true validity of the corrected age estimates is open to question but is illustrative of the probable cause of the age disagreement with the radiocarbon data. As a result of the uncertainties surrounding the OSL chronology this has been excluded from subsequent interpretation and discussion.

Palaeotemperature

Mean annual palaeotemperatures were calculated following Goodwin et al. (2003) using the equation: temperature = 20.6 – 4.34 [$\delta^{18}O_{aragonite}$ – ($\delta^{18}O_{water}$ - 0.2)] (Table 4). A value of +3 ‰ was applied for $\delta^{18}O_{water}$ in accordance with the relationships observed from the analysis of Recent marine water samples taken from offshore Abu Dhabi (Lokier and Steuber, 2009). The two *Pinctada* specimens yielded palaeotemperatures of 27.7°C and 30.5°C while the *Barbatia* specimen yielded a palaeotemperature of 22.6°C (Table 4). The differences in these results are reconcilable as *Pinctada* are often associated with mid to lower shore settings while *Barbatia* is associated with deeper, lower shore to sublittoral, environments (Bosch et al., 1995). These temperatures are entirely consistent with the temperatures observed along the coastline of Abu Dhabi today with surface temperatures ranging between 22-37°C (Evans et al., 1973) while temperatures below 4-5 m water depth range between 20-36°C (Kinsman, 1964).

Interpretation and discussion

Palaeoenvironmental context of the skeleton

The siliciclastic material within the lowermost units of the sedimentary sequence is inferred to have been derived from the underlying quartz-rich sands as documented by Kirkham (1998). These sands have previously been interpreted as being deposited as aeolian dunes and are dated from prior to the post-glacial reflooding of the Persian Gulf (Evans et al., 1969) with ages between 26,760 (±180) ^{14}C yrs BP and 24,010 (±150) ^{14}C yrs BP proposed by Strohmenger et al. (2010). However, as these dates are derived from bulk samples of sediment, they should be treated with a degree of caution as there is a strong likelihood of the samples being contaminated with carbonate material from a wide range of sources and with a wide range of ages. During transgression these aeolian sands were locally eroded and admixed into the overlying transgressive quartz-rich carbonate unit.

The overlying microbial mat (Fig. 2) has previously been interpreted as a transgressive unit (Kenig et al., 1990). Recent microbial mat communities are well-developed in the Recent Abu Dhabi sabkha where they form a belt marking the landward-limit of the intertidal zone (Lokier and Steuber, 2008). At this position, brief periods of flooding prevent complete desiccation of the mats whilst regular exposure inhibits predation by grazing marine gastropods. The microbial mat horizon observed in the Mussafah Channel section is here inferred to record a similar stressed upper intertidal environment. Its stratigraphic position, immediately overlying the transgressive quartz-rich carbonate sands, is consistent with a slowing in transgression or a stillstand.

In the Recent Abu Dhabi sabkha the microbial mats are typically only 1-5 cm in thickness. The development of thicker microbial mats is limited to depressions in the upper intertidal zone where water is able to pond following spring high tides. Evaporation from these ponds results in elevated salinities that prohibit colonisation by grazing fauna, thereby allowing successive generations of microbial mat to build laminated units until the ponds are infilled. The microbial mat observed in the Mussafah Channel section is 11 cm in thickness (Fig. 2). This may be attributed to the flooding of antecedent dune topography followed by a stillstand. Subtle variations in relief would result in local variations in water depth with isolated shallow basins permitting the development of locally thicker microbial mat units.

The hardground that immediately overlies the microbial mats (Fig. 2) is interpreted to have developed in the lower intertidal to subtidal zone, a setting in which hardgrounds are developing in the Persian Gulf today (Lokier and Steuber, 2009; Shinn, 1969). This implies renewed transgression following deposition of the microbial mat horizon (Fig. 6). The preservation of the underlying microbial mats during transgression is problematic since marine flooding will place the mats in an environment where gastropods or other marine organisms are able to actively graze upon them. However, if transgression was rapid, then it is feasible that the microbial mats would be promptly buried, thus preserving them from grazing epifauna. Buried mats would remain vulnerable to destruction through the activities of burrowing deposit-feeding organisms. However, the modern microbial mats are observed to be anoxic at shallow depths below the surface. Such anoxia would inhibit infaunal activity. The development of hardgrounds can be rapid, crusts may form in less than 20 years (Shinn, 1969), thus aiding the preservation of underlying microbial mats.

Recent intertidal hardgrounds form large-scale (>100 m diameter) polygons with a dish-like morphology comprising a planar interior and gently-uplifted margins. The polygons retain water to form shallow (10 cm) ponds at low tide and are totally inundated, and recharged, during high tides. The interior of these intertidal polygons is covered by a thin (3-5 cm) veneer of sediment that may be temporarily removed during high-energy storm events (Lokier and Steuber, 2009). Beneath this veneer is a poorly-lithified firmground of 1-4 cm thickness that represents the zone of active cementation (Lokier and Steuber, 2009). Beneath the firmground is the hardground proper. The presence of the unlithified sediment veneer prohibits encrustation by benthic communities over most of the hardground surface; encrustation is limited to the exposed uplifted polygon margins where a diverse range of benthos is observed.

The lower portions of the cetacean jaws and skull are locally embedded within the hardground; the cetacean must therefore have been emplaced into the intertidal zone prior to the completion of lithification. As the bones do not completely penetrate through the hardground, it is likely that the hardground had already begun to lithify prior to the arrival of the cetacean. Following arrival, the heavier bones of the jaw and skull would have penetrated into the firmground to become cemented during continued hardground development. The presence of encrusting benthos on the low-lying bones proves that the lower portion of these bones must have been regularly submerged and supports the interpretation of emplacement of the cetacean onto a shallow, lower intertidal hardground pond. The interpretation of emplacement of the whale into a shallow intertidal hardground pond is supported by the low-diversity of the ostracod assemblage as previously documented from the Mussafah Channel (Stewart et al., 2011) as these ponds are known to have high salinities today.

Previous studies have hypothesised that the cetacean was emplaced into a tidal channel (Stewart et al., 2011; Strohmenger et al., 2010). However, we do not support this interpretation for the following reasons: 1) Tidal channels typically concentrate water flow during the ebb tide; therefore they are a focus of off-shore transport. As such, it is unlikely that, once emplaced, a carcass would remain for very long in such a setting. 2) Tidal channels are high-energy features, typically with erosive bases. There is no evidence of an erosive base at the whale excavation site. 3) The high energies that are typical of tidal channels would rapidly disarticulate the skeleton and transport the smaller bones, such as the phalanges, offshore. 4) The presence of coarse-grained bioclastic material banked against the bones is unlikely to occur in a tidal channel where such material is easily transported off-shore. 5) Any hard substrates in channels are heavily encrusted by marine benthos yet only the lowermost portions of the skeleton were encrusted.

The remarkably planar surface of the hardground in the Mussafah Channel (Fig. 4) has previously been interpreted as a possible aeolian erosional feature in which the surface of the hardground was wind-planed (Kirkham, 1998). However, as some of the cetacean bones clearly penetrate, and are cemented within, the hardground this interpretation is deemed to be unlikely, as such an intense process would have caused significant abrasion and, weathering of the skeleton.

The excellent state of preservation and relatively complete articulation of the bones is consistent with relatively rapid burial following emplacement. The stratigraphic sequence overlying the hardground, and containing the cetacean skeleton, exhibits an overall fining-upward trend (Figs 2 and 5) that implies a reduction in energy regimes consistent with deepening of the palaeoenvironment during continued transgression. This subtidal sequence differs significantly from the progradational sedimentary sequence described previously from elsewhere in the Abu Dhabi sabkha (Evans et al., 1969; Kirkham, 1998; Lokier and Steuber, 2008). Of particular interest is the lack of a microbial mat horizon at the contact between the carbonate-dominated intertidal sediments and the overlying supratidal evaporite-dominated units in the Mussafah Channel section. As mentioned previously, microbial mats demark the uppermost intertidal zone and, during progradation, are likely to be preserved, even following shallow burial, on entering the supratidal environment. Their absence from the Mussafah Channel section is consistent with a rapid fall in sea level resulting in rapid progradation of the shoreline without allowing sufficient time for significant microbial mat development. The succeeding, laterally discontinuous, peloidal and skeletal muddy sand horizons are inferred to represent the abandonment of storm-surge emplaced beach ridges during this regression. The uppermost unit in the sequence records the displacive growth of gypsum, and near-surface anhydrite, in a supratidal sabkha setting.

The bioclast-rich sandy gravels banked against the bones are inferred to have been transported and deposited during storm surges. The accumulation of coarse-grained sediments against obstructions is a common feature in the intertidal zone of the Recent sabkha of Abu Dhabi. As these bioclasts are transported and are, thus, not *in situ*, they can not be directly employed in the palaeoenvironmental analysis of the depositional environment of the skeleton. However, the diverse assemblage, as documented by Stewart et al. (2011) is consistent with the range of environments, from hypersaline intertidal to less-saline shallow subtidal settings associated with the Recent coastline of Abu Dhabi.

The thin sub-vertical burrows observed in the subtidal sequence have previously been interpreted as rootlets produced by seagrass and, as such, have been posited as evidence of a lagoonal environment (Strohmenger et al., 2010). These features are, in fact, the mm-diameter, mucus-lined burrows of an arthropod of the class arachnida. This mite produces identical burrows in the supratidal zone of the Recent Abu Dhabi sabkha. As these burrows cross-cut stratigraphy they are not strictly diagnostic of the facies in which they occur.

A siliciclastic component is relatively common within the Recent sediments of the Abu Dhabi shoreline. This material is primarily derived from subaerially-exposed erosional remnants of the middle-late Pleistocene Ghayathi Formation in the supratidal zone and generally reduces in abundance distally into the lower intertidal to subtidal zone (Lokier et al., 2013). The lack of siliciclastic material in the units associated with, and immediately overlying, the skeleton (Fig. 5) is consistent with deposition in a setting at some distance from the supratidal zone.

The laterally-continuous iron oxide-stained horizons (Fig. 2) have previously been interpreted as marking the positions of a fluctuating groundwater table (Kirkham, 1998).

The skeleton's location in relation to the present day coastline infers a minimum progradation of the coast of 8.3 km since the whale was deposited, this equates to a progradation rate of between 1.56-1.81 m/yr. This progradation rate lies within the range of 1.5-2 m/yr proposed from previous studies of the sabkha system (Kenig, 1991; Kinsman and Park, 1976; Patterson and Kinsman, 1977; Warren, 2006) but is significantly higher than an average rate of 0.75 m/yr as previously proposed for the more recent, post 1.4 ka, seaward portion of the sabkha system (Lokier and Steuber, 2008). This disparity is consistent with the slowing of progradation rates over time, implying rates exceeding

1.81 m/yr prior to 1.4 ka. A rapid fall in sea level resulted in forced regression that was followed by normal progradation as sea levels stabilised at a lower level (Fig. 6).

Implications for mid- to late Holocene relative sea level

The sedimentary sequence observed at the Mussafah Channel is interpreted in the context of a whale beaching event as a complete parasequence recording a single flooding episode followed by a relative sea level fall. As mentioned previously, the microbial mat belt in the Recent Abu Dhabi sabkha is constrained to the landward limit of the intertidal zone, and is therefore effectively a datum recording the height of mean higher high water (MHHW). We can assume that the buried, ancient, microbial mat observed in the Mussafah Channel stratigraphic section was developed in a similar environment and, thus, records MHHW at the time of microbial mat growth. Today, the height of MHHW for the Umm Al Nar tide gauge (Fig. 1) is 1.64 m (Mohamed, 2008). The ancient microbial mat at the Mussafah Channel section lies at 1.85 m above chart datum, it can therefore be inferred that sea levels were 20 cm higher than today at 7103-6887 cal yr BP (Fig. 6). The effect of post-depositional compaction on a sedimentary section of approximately 1 m thickness would be negligible (Brain et al., 2012), however, it remains possible that the actual sea level was slightly in excess of 20 cm.

The succession of the microbial mat by a hardground horizon records a retrogradational geometry during continued flooding from 6887-6567 cal yr BP, with an additional 1.1 m of carbonate and evaporite sediments being deposited above the microbial mat (Fig. 2). In peritidal carbonate settings it has been inferred that accommodation space will be completely infilled by sediments (Fischer, 1964) however recent research has called this traditional ‘accommodation filling’ view into doubt (Boss and Rasmussen, 1995; Eberli, 2013; Wilkinson et al., 1997). It is now recognised that accommodation space is filled irregularly, this is due to the off-bank transport of carbonate material by tides, wave currents and storms (Eberli, 2013). Given these factors, along with the unknown degree of compaction, it is unlikely that the 1.3 m of section that lies above current MHHW accurately records the true amplitude of the late Holocene sea level highstand. Instead, this figure should be considered as a minimum value for the highstand (Fig. 6).

A further complicating factor in estimating the amplitude of the late Holocene highstand is the displacive growth of evaporite minerals in the sedimentary column. In the Mussafah Channel setting, between 26 to 34 cm thickness of evaporite-dominated sediments are recorded (Figs 2 & 5). These units have developed through displacive interstitial growth in the supratidal setting and have therefore increased the thickness of the sediment pile by approximately 30 cm. A final complicating factor in estimating the late Holocene highstand is that, following sea level fall, after 5285-4574 cal yr BP, it is likely that the sediment pile was deflated to within 50 cm of the groundwater table, as is observed in the Abu Dhabi sabkha today.

Previous dates for the timing of the late Holocene highstand at the Abu Dhabi shoreline have varied widely. The transgressive phase has been dated as exceeding current sea levels at between 7000 - 6000 BP (Evans et al., 1969; Lambeck, 1996) and reaching a maximum of 1-2 m above current sea level (Evans et al., 1973; Kenig, 1991; Lambeck, 1996; Uchupi et al., 1996; Williams and Walkden, 2002) by between 6000-3400 BP (Evans et al., 1973; Evans et al., 1969; Kenig, 1991; Uchupi et al., 1996; Williams and Walkden, 2002). Sea level fall has been dated as commencing between 4500-2300 BP (Evans et al., 1969; Uchupi et al., 1996; Williams and Walkden, 2002) and reached current levels by 1600-1000 BP (Kenig, 1991; Uchupi et al., 1996). The large discrepancies between these dates may be attributed to the wide variety of material selected for radiocarbon dating. Many of the studies employed bulk sediment samples or the shells of detrital feeding organisms as the source of carbon, both of which are inherently unreliable for dating. A further source of error is that none of these studies undertook a calibration of the radiocarbon ages in order to take account of the marine reservoir effect.

An additional complication to the Quaternary history of the Persian Gulf has recently been introduced by Wood et al. (2012) who have proposed a tectonic uplift of 125 m over the last 18 ka, with current uplift rates of 1 mm/yr. Given that the relief of the Mussafah Channel microbial mat is akin to present day MHHW, such a rate of tectonic uplift would necessitate a eustatic sea level rise of 7 m over the past 7,000 years with a stillstand in the shoreline of the Persian Gulf over this period – a hypothesis that clearly is not supported by any observational evidence, both in this study and elsewhere. Thus, our observations support the hypothesis that the southern shore of the Persian Gulf has been tectonically stable throughout the late Quaternary (Stevens et al., 2014).

In conclusion, the mid- to late Holocene sea level highstand surpassed present day sea level at 7100-6890 cal yr BP and reached a minimum amplitude of 1 m above current sea level (Fig. 6). Unfortunately, due to a lag in sediment deposition and the effects of deflation, it is not possible to constrain the upper limit or the exact timing of this sea level peak other than stating that this must have occurred after 5290-4570 cal yr BP. On the basis of previous observations of the progradational sabkha sequence (Lokier and Steuber, 2008) it is inferred that sea level had fallen to near current levels by 1440-1170 cal yr BP.

Regional and global context

The new results from the United Arab Emirates place accurate constraints as to the timing of the transgressive, highstand and regressive episodes associated with the mid- to late Holocene sea level high, both in the context of the Persian Gulf and at a broader, global, perspective. Although the timing and elevation of the Holocene highstand has been reported as varying both spatially and temporally (Murray-Wallace, 2007) these new results are comparable to those observed elsewhere throughout the Indian Ocean region (Table 5) (Horton et al., 2005; Kench et al., 2009; Ramsay, 1996; Ranasinghe et al., 2013; Woodroffe and Horton, 2005). Small disparities in the timing (on the scale of a few hundreds of years) and amplitude (by up to +2 m) of the highstand between these areas are inferred to result from hydro-isostatic effects and mantle rheology (Milne et al., 2009; Stattegger et al., 2013; Woodroffe and Horton, 2005).

These new limits as to the timing of the mid- to late Holocene sea level highstand in the Persian Gulf also compares favourably with previously proposed, though, often, less well-constrained, dates for the transgressive and regressive phases from SE Asia (Chappell and Polach, 1991; Geyh et al., 1979; Scoffin and Le Tissier, 1998; Stattegger et al., 2013; Tjia, 1996; Woodroffe and McLean, 1990; Yim and Huang, 2002), Australia (Baker and Haworth, 2000; Baker et al., 2001; Beaman et al., 1994; Collins et al., 2006; Flood and Frankel, 1989), the Pacific (Grossman et al., 1998; Nunn and Peltier, 2001) and the Atlantic (Angulo et al., 2006; Bourrouilh-Le Jan, 2007; Compton, 2001; Gayes et al., 1992; van Soelen et al., 2010) regions (Table 5).

Many of these previous studies have been unable to decouple proposed eustatic sea level changes from the signature of local and far field tectonic adjustments (Milne et al., 2009). The tectonically stable southern shoreline of the Persian Gulf (Stevens et al., 2014) has not been affected either by glacio-isostatic adjustment or by the far field effects of isostatic loading. We are therefore able to confidentially establish that the mid- to late Holocene sea level history of the Persian Gulf is driven by eustatic sea level without any influence from regional tectonic events.

Conclusions

The data from this study refine our knowledge of the timing of the transgression and regression phases associated with the global mid- to late Holocene sea level highstand. We establish that mid-Holocene transgression exceeded present day sea level by 7100-6890 cal yr BP with a highstand of > 1 m above current seal level being reached shortly after 5290-4570 cal yr BP. Subsequent relative sea level fall had attained current datum by 1440-1170 cal yr BP. These new dates allow us to hone previously-defined dates for the mid- to late Holocene sea level highstand from other regions, thereby constraining the timing of this correlatable global eustatic event.

The Mussafah Channel cetacean was emplaced during the mid-Holocene transgressive phase, being beached between 5300-4960 cal yr BP into an intertidal hardground pond. Paleoenvironmental regimes in this setting, in terms of temperature, salinity and energy, are inferred to have been akin to those observed at the coastline of Abu Dhabi today. Continued transgression saw the burial of the skeleton within shallow-subtidal sediments before the relative sea level fall resulted in a forced regression and a consequent rapid progradation in facies. We infer that the southern shoreline of the Persian Gulf was tectonically stable at this time with relative sea level being driven by global eustasy.

This study also illustrates the potential pitfalls of applying optically stimulated luminescence dating techniques in isolation within sabkha environments. In arid coastal environments a high evaporation rate in association with fluctuating saline groundwater levels may result in leaching and concentration of uranium and potassium with consequent post-burial modifications of the environmental radiation dose. Thus, measured elemental concentrations may not reflect the average concentrations during the burial history of the sediments. This finding has important implications for studies in similar settings where optically stimulated luminescence may be employed as the sole dating method.

Acknowledgements

We thank ADACH, ADNOC and EAD for logistical and financial support during the fieldwork. Associate Editor Dr Curtis W. Marean and reviewer Dr Charlotte Schreiber are thanked for their astute comments and suggestions that, we believe, have enhanced the quality of this manuscript. SL also thanks Ali AL-Kaabi for assistance in the field and making his samples available for analysis.

References

Angulo, R.J., Lessa, G.C., Souza, M.C.d., 2006. A critical review of mid- to late-Holocene sea-level fluctuations on the eastern Brazilian coastline. Quaternary Science Reviews 25, 486-506.

Baker, R.G.V., Haworth, R.J., 2000. Smooth or oscillating late Holocene sea-level curve? Evidence from the palaeo-zoology of fixed biological indicators in east Australia and beyond. Marine Geology 163, 367-386.

Baker, R.G.V., Haworth, R.J., Flood, P.G., 2001. Inter-tidal fixed indicators of former Holocene sea levels in Australia: a summary of sites and a review of methods and models. Quaternary International 83–85, 257-273.

Banerjee, D., Murray, A.S., Bøtter-Jensen, L., Lang, A., 2001. Equivalent dose estimation using a single aliquot of polymineral fine grains. Radiation Measurements 33, 73-94.

Bateman, M.D., Boulter, C.H., Carr, A.S., Frederick, C.D., Peter, D., Wilder, M., 2007. Detecting post-depositional sediment disturbance in sandy deposits using optical luminescence. Quaternary Geochronology 2, 57-64.

Beaman, R., Larcombe, P., Carter, R.M., 1994. New evidence for the Holocene sea-level high from the inner shelf, central Great Barrier Reef, Australia. Journal of Sedimentary Research 64, 881-885.

Bosch, D.T., Dance, S.P., Moolenbeek, R.G., Oliver, P.G., 1995. Seashells of Eastern Arabia. Motivate Publishing, Dubai.

Boss, S.K., Rasmussen, K.A., 1995. Misuse of Fischer plots as sea-level curves. Geology 23, 221-224.

Bottomley, N., 1996. Recent climate of Abu Dhabi, in: Osborne, P.E. (Ed.), Desert ecology of Abu Dhabi. A review and recent studies. Pisces, Newbury, pp. 36-49.

Bourrouilh-Le Jan, F.G., 2007. Very high energy sedimentation (supratidal hurricane deposits) and Mid-Holocene highstand on carbonate platforms, Andros, Bahamas: An alternative view. Sedimentary Geology 199, 29-49.

Brain, M.J., Long, A.J., Woodroffe, S.A., Petley, D.N., Milledge, D.G., Parnell, A.C., 2012. Modelling the effects of sediment compaction on salt marsh reconstructions of recent sea-level rise. Earth and Planetary Science Letters 345-348, 180-193.

Cazenave, A., Nerem, R.S., 2004. Present-day sea level change: Observations and causes. Rev. Geophys. 42, RG3001.

Chappell, J., Polach, H., 1991. Post-glacial sea-level rise from a coral record at Huon Peninsula, Papua New Guinea. Nature 349, 147-149.

Clark, P.U., Dyke, A.S., Shakun, J.D., Carlson, A.E., Clark, J., Wohlfarth, B., Mitrovica, J.X., Hostetler, S.W., McCabe, A.M., 2009. The Last Glacial Maximum. Science 325, 710-714.

Collins, L.B., Zhao, J.-X., Freeman, H., 2006. A high-precision record of mid–late Holocene sea-level events from emergent coral pavements in the Houtman Abrolhos Islands, southwest Australia. Quaternary International 145–146, 78-85.

Compton, J.S., 2001. Holocene sea-level fluctuations inferred from the evolution of depositional environments of the southern Langebaan Lagoon salt marsh, South Africa. The Holocene 11, 395-405.

Eberli, G.P., 2013. The uncertainties involved in extracting amplitude and frequency of orbitally driven sea-level fluctuations from shallow-water carbonate cycles. Sedimentology 60, 64-84.

Evans, G., Murray, J.W., Biggs, H.E.J., Bate, R., Bush, P.R., 1973. The oceanography, ecology, sedimentology and geomorphology of parts of the Trucial Coast barrier island complex, Persian Gulf, in: Purser, B.H. (Ed.), The Persian Gulf - Holocene Carbonate Sedimentation and Diagenesis in a Shallow Epicontinental Sea. Springer-Verlag, Berlin, pp. 233-277.

Evans, G., Schmidt, V., Bush, P., Nelson, H., 1969. Stratigraphy and geologic history of the sabkha, Abu Dhabi, Persian Gulf. Sedimentology 12, 145-159.

Fischer, A.G., 1964. The Lofer Cyclothems of the Alpine Triassic. Kansas Geological Survey, Bulletin 169, 107-149.

Fleming, K., Johnston, P., Zwartz, D., Yokoyama, Y., Lambeck, K., Chappell, J., 1998. Refining the eustatic sea-level curve since the Last Glacial Maximum using far- and intermediate-field sites. Earth and Planetary Science Letters 163, 327-342.

Flood, P.G., Frankel, E., 1989. Late Holocene higher sea level indicators from eastern Australia. Marine Geology 90, 193-195.

Galbraith, R.F., Green, P.F., 1990. Estimating the component ages in a finite mixture. International Journal of Radiation Applications and Instrumentation. Part D. Nuclear Tracks and Radiation Measurements 17, 197-206.

Gayes, P.T., Scott, D.B., Collins, E.S., Nelson, D.D., 1992. A Late Holocene sea-level fluctuation in South Carolina, in: Fletcher III, C.H., Wehmiller, J.F. (Eds.), Quaternary coasts of the United States: Marine and Lacustrine Systems. SEPM, pp. 155-160.

Geyh, M.A., Streif, H., Kudrass, H.R., 1979. Sea-level changes during the late Pleistocene and Holocene in the Strait of Malacca. Nature 278, 441-443.

Goodwin, D.H., Schone, B.R., Dettman, D.L., 2003. Resolution and Fidelity of Oxygen Isotopes as Paleotemperature Proxies in Bivalve Mollusk Shells: Models and Observations. PALAIOS 18, 110-125.

Grossman, E.E., Fletcher Iii, C.H., Richmond, B.M., 1998. The Holocene sea-level highstand in the equatorial Pacific: analysis of the insular paleosea-level database. Coral Reefs 17, 309-327.

Hanebuth, T.J.J., Stattegger, K., Bojanowski, A., 2009. Termination of the Last Glacial Maximum sea-level lowstand: The Sunda-Shelf data revisited. Global and Planetary Change 66, 76-84.

Horton, B.P., Gibbard, P.L., Mine, G.M., Morley, R.J., Purintavaragul, C., Stargardt, J.M., 2005. Holocene sea levels and palaeoenvironments, Malay-Thai Peninsula, southeast Asia. The Holocene 15, 1199-1213.

Hughen, K.A., Baillie, M.G.L., Bard, E., Bayliss, A., Beck, J.W., Bertrand, C.J.H., Blackwell, P.G., Buck, C.E., Burr, G.S., Cutler, K.B., Damon, P.E., Edwards, R.L., Fairbanks, R.G., Friedrich, M., Guilderson, T.P., Kromer, B., McCormac, F.G., Manning, S.W., Bronk Ramsey, C., Reimer, P.J., Reimer, R.W., Remmele, S., Southon, J.R., Stuiver, M., Talamo, S., Taylor, F.W., van der Plicht, J., Weyhenmeyer, C.E., 2004. Marine04 Marine radiocarbon age calibration, 26 - 0 ka BP. Radiocarbon 46, 1059-1086.

Kench, P.S., Smithers, S.G., McLean, R.F., Nichol, S.L., 2009. Holocene reef growth in the Maldives: Evidence of a mid-Holocene sea-level highstand in the central Indian Ocean. Geology 37, 455-458.

Kenig, F., 1991. Sédimentation, distribution et diagenèse de la matière organique dans un environment carbonaté hypersalin: le système lagune-sabkha d'Abu Dhabi, Institut Français du Pétrole. Université d'Orléans, France, p. 328.

Kenig, F., Huc, A.Y., Purser, B.H., Oudin, J.L., 1990. Sedimentation, distribution and diagenesis of organic-matter in a recent carbonate environment, Abu-Dhabi, UAE. Organic Geochemistry 16, 735-747.

Kinsman, D.J.J., 1964. Reef coral tolerance of high temperature and salinites. Nature, 1280-1282.

Kinsman, D.J.J., Park, R.K., 1976. Algal belt and coastal sabkha evolution, Trucial Coast, Persian Gulf, in: Walter, M.H. (Ed.), Stromatolites. Elsevier, pp. 421-433.

Kirkham, A., 1998. A Quaternary proximal foreland ramp and its continental fringe, Arabian Gulf, UAE, in: Wright, V.P., Burchette, T.P. (Eds.), Carbonate Ramps. Geological Society, London, pp. 15-41.

Lambeck, K., 1996. Shoreline reconstructions for the Persian Gulf since the last glacial maximum. Earth and Planetary Science Letters 142, 43-57.

Leuliette, E., Nerem, R., Mitchum, G., 2004. Calibration of TOPEX/Poseidon and Jason Altimeter Data to Construct a Continuous Record of Mean Sea Level Change. Marine Geodesy 27, 79-94.

Lian, O.B., Hu, J., Huntley, D.J., Hicock, S.R., 1995. Optical dating studies of Quaternary organic-rich sediments from southwestern British Columbia and northwestern Washington State. Canadian Journal of Earth Sciences 32, 1194-1207.

Lokier, S., Steuber, T., 2008. Quantification of carbonate-ramp sedimentation and progradation rates for the late Holocene Abu Dhabi shoreline. Journal of Sedimentary Research 78, 423-431.

Lokier, S., Steuber, T., 2009. Large-scale intertidal polygonal features of the Abu Dhabi coastline. Sedimentology 56, 609-621.

Lokier, S.W., 2012. Development and evolution of subaerial halite crust morphologies in a coastal sabkha setting. Journal of Arid Environments 79, 32-47.

Lokier, S.W., Knaf, A., Kimiagar, S., 2013. A quantitative analysis of Recent arid coastal sedimentary facies from the Arabian Gulf Coastline of Abu Dhabi, United Arab Emirates. Marine Geology 346, 141-152.

Milne, G.A., Gehrels, W.R., Hughes, C.W., Tamisiea, M.E., 2009. Identifying the causes of sea-level change. Nature Geosci 2, 471-478.

Mohamed, K.A., 2008. Long-term tidal water level measurements in Abu Dhabi Emirate, ASME 27th International Conference on Offshore Mechanics and Arctic Engineering. ASME, Estoril, Portugal, pp. 937-944.

Murray-Wallace, C.V., 2007. Eustatic sea-level chnages since the last glaciation, in: Ellias, S.A. (Ed.), Encyclopedia of Quaternary Science. Elsevier, Amsterdam, pp. 3034-3043.

Murray, A.S., Wintle, A.G., 2000. Luminescence dating of quartz using an improved single-aliquot regenerative-dose protocol. Radiation Measurements 32, 57-73.

Nunn, P.D., Peltier, W.R., 2001. Far-Field Test of the ICE-4G Model of Global Isostatic Response to Deglaciation Using Empirical and Theoretical Holocene Sea-Level Reconstructions for the Fiji Islands, Southwestern Pacific. Quaternary Research 55, 203-214.

Patterson, R.J., Kinsman, D.J.J., 1977. Marine and continental groundwater sources in a Persian Gulf coastal sabkha, Reefs and Related Carbonates - Ecology and Sedimentology. AAPG, pp. 381-397.

Peltier, W.R., Fairbanks, R.G., 2006. Global glacial ice volume and Last Glacial Maximum duration from an extended Barbados sea level record. Quaternary Science Reviews 25, 3322-3337.

Prescott, J.R., Hutton, J.T., 1994. Cosmic ray contributions to dose rates for luminescence and ESR dating: Large depths and long-term time variations. Radiation Measurements 23, 497-500.

Purser, B.H., Evans, G., 1973. Regional sedimentation along the Trucial Coast, SE Persian Gulf, in: Purser, B.H. (Ed.), The Persian Gulf - Holocene Carbonate Sedimentation and Diagenesis in a Shallow Epicontinental Sea. Springer-Verlag, Berlin, pp. 211-231.

Raafat, H., 2007. Climate, in: Kumar, A. (Ed.), Physical Geography Sector Paper. Environment Agency Abu Dhabi, pp. 72-89.

Ramsay, P.J., 1996. 9000 Years of sea-level change along the southern African coastline. Quaternary International 31, 71-75.

Ranasinghe, P.N., Ortiz, J.D., Moore, A.L., McAdoo, B., Wells, N., Siriwardana, C.H.E.R., Wijesundara, D.T.D.S., 2013. Mid–Late Holocene coastal environmental changes in southeastern Sri Lanka: New evidence for sea level variations in southern Bay of Bengal. Quaternary International 298, 20-36.

Sarnthein, M., 1972. Sediments and history of the Postglacial transgression in the Persian Gulf and northwest Gulf of Oman. Marine Geology 12, 245-266.

Scoffin, T.P., Le Tissier, M.D.A., 1998. Late Holocene sea level and reef flat progradation, Phuket, South Thailand. Coral Reefs 17, 273-276.

Shinn, E.A., 1969. Submarine lithification of Holocene carbonate sediments in the Persian Gulf. Sedimentology 12, 109-144.

Stattegger, K., Tjallingii, R., Saito, Y., Michelli, M., Trung Thanh, N., Wetzel, A., 2013. Mid to late Holocene sea-level reconstruction of Southeast Vietnam using beachrock and beach-ridge deposits. Global and Planetary Change 110, Part B, 214-222.

Stevens, T., Jestico, M.J., Evans, G., Kirkham, A., 2014. Eustatic control of late Quaternary sea-level change in the Arabian/Persian Gulf. Quaternary Research 82, 175-184.

Stewart, J.R., Aspinall, S., Beech, M., Fenberg, P., Hellyer, P., Larkin, N., Lokier, S.W., Marx, F.G., Meyer, M., Miller, R., Rainbow, P.S., Taylor, J.D., Whittaker, J.E., Al-Mehsin, K., Strohmenger, C.J., 2011. Biotically constrained palaeoenvironmental conditions of a mid-Holocene intertidal lagoon on the southern shore of the Arabian Gulf: evidence associated with a whale skeleton at Musaffah, Abu Dhabi, UAE. Quaternary Science Reviews 30, 3675-3690.

Strohmenger, C.J., Al-Mansoori, A., Al-Jeelani, O., Al-Shamry, A., Al-Hosani, I., Al-Mehsin, K., Shebl, H., 2010. The sabkha sequence at Mussafah Channel (Abu Dhabi, United Arab Emirates): Facies stacking patterns, microbial-mediated dolomite and evaporite overprint. GeoArabia 15, 49-90.

Stuiver, M., Polach, H.A., 1977. Discussion reporting of 14C data. Radiocarbon 19, 355-363.

Stuiver, M., Reimer, P.J., 1993. Extended 14C database and revised CALIB radiocarbon calibration program. Radiocarbon 35.

Taylor, S.R., McClennan, S.M., 1985. The continental crust: Its composition and evolution. Blackwell Scientific Publications, Oxford.

Tjia, H.D., 1996. Sea-level changes in the tectonically stable Malay-Thai Peninsula. Quaternary International 31, 95-101.

Uchupi, E., Swift, S.A., Ross, D.A., 1996. Gas venting and late Quaternary sedimentation in the Persian (Arabian) Gulf. Marine Geology 129, 237-269.

van Soelen, E.E., Lammertsma, E.I., Cremer, H., Donders, T.H., Sangiorgi, F., Brooks, G.R., Larson, R.A., Sinninghe Damsté, J.S., Wagner-Cremer, F., Reichart, G.J., 2010. Late Holocene sea-level rise in Tampa Bay: Integrated reconstruction using biomarkers, pollen, organic-walled dinoflagellate cysts, and diatoms. Estuarine, Coastal and Shelf Science 86, 216-224.

Walker, M., 2005. Quaternary Dating Methods. John Wiley & Sons, Ltd.

Warren, J.K., 2006. Evaporites: Sediments, Resources and Hydrocarbons. Pringer.

Wilkinson, B.H., Drummond, C.N., Rothman, E.D., Diedrich, N.W., 1997. Stratal order in peritidal carbonate sequences. Jounrnal of Sedimentary Research 67, 1068-1082.

Williams, A.H., Walkden, G.M., 2002. Late Quaternary highstand deposits of the southern Arabian Gulf: a record of sea-level and climate change, in: Clift, P.D., Kroon, D., Gaedicke, C. & Craig, J. (Ed.), The Tectonic and Climatic Evolution of the Arabian Sea Region. Geological Society of London, London, pp. 371-386.

Wilson, P., Vincent, P.J., Telfer, M.W., Lord, T.C., 2008. Optically stimulated luminescence (OSL) dating of loessic sediments and cemented scree in northwest England. The Holocene 18, 1101-1112.

Wood, W.W., Bailey, R.M., Hampton, B.A., Kraemer, T.F., Lu, Z., Clark, D.W., James, R.H.R., Al Ramadan, K., 2012. Rapid late Pleistocene/Holocene uplift and coastal evolution of the southern Arabian (Persian) Gulf. Quaternary Research 77, 215-220.

Woodroffe, C., McLean, R., 1990. Microatolls and recent sea level change on coral atolls. Nature 344, 531-534.

Woodroffe, S.A., Horton, B.P., 2005. Holocene sea-level changes in the Indo-Pacific. Journal of Asian Earth Sciences 25, 29-43.

Yim, W.W.S., Huang, G., 2002. Middle Holocene higher sea-level indicators from the south China coast. Marine Geology 182, 225-230.

Yokoyama, Y., Lambeck, K., De Deckker, P., Johnston, P., Fifield, L.K., 2000. Timing of the Last Glacial Maximum from observed sea-level minima. Nature 406, 713-716.

List of Tables

1 Modal analysis results for the sediment samples.

2 Radiocarbon ages, calibrated age ranges (2σ), and calculated progradation rates from this study.

3 OSL age estimates for samples analysed in this study.

4 Stable isotope analysis results and calculated palaeotemperatures of the studied samples. Palaeotemperatures were calculated following Goodwin et al. (2003).

5 Previously reported dates of transgressive, highstand and regressive phases along with maximum sea level heights for the mid- to late Holocene highstand.

List of Figures

1 Map of the Persian Gulf region. The dashed box indicates the location of Fig. 1 B. B) Detailed map showing the location of the Mussafah Channel.

2 Lithostratigraphic logs of the three sections logged in detail during the study. The stratigraphic position of OSL samples is displayed against section MC1.The location of section MC-3 is indicated on the site plan (Fig. 3). Coordinates are to map datum WGS 84.

3 Plan of the cetacean bones excavated at the Mussafah Channel site showing the relationship between the bones and the associated samples used in radiocarbon and stable isotope analysis. Note the location of logged section MC-3 at grid reference 4.0, 7.5. Grids are at 0.5 m intervals referenced to site datum. Site plan by P. Rye, drafted by A.C. Lokier.

4 A) General overview of the excavation site showing the location of logged section MC-3 and the extremely planar surface of the hardground (HG). Photograph of logged section MC-3, highlighting the location of the enterolithic anhydrite (e) and the prominent iron stained horizon (Fe). Note the large bone covered in plaster of Paris (b) in the lower left corner of the section. Image A courtesy Nigel Larkin.

5 The relationship between sedimentary facies and component allochems for the three logged sections.

6 Relative sea level trends and relationships to the depositional facies observed within the Mussafah Channel sequence.

Table 1

	Components																	
Section	Depth (cm)	Peloid	Ooid	Mud	Gypsum grain	Anhydrite	Quartz	Feldspar	Lithic grain	Calcite cement	Gypsum cement	Foraminifera	Bivalve	Gastropod	Echinoid	Ostracod	Bryozoan	Unidentified bioclast
	7	3.0				95.5										1.0		0.5
	19	23.0		62.0		13.5												1.5
	34	43.5		37.0	3.0							1.5				2.0		13.0
	53			84.0	6.0							1.5				1.0		7.5
MC1	65	12.0		85.0	2.0											0.5		0.5
	95	51.4		32.9	1.3									12.7				1.7
	105	27.3	0.3	17.7	1.8		1.8			15.5		2.4	1.8	21.6		0.3		9.5
	113	16.5		67.5	4.5		1.5		2.0									8.0
	131	33.2		26.9	9.0		1.0	1.0	3.0			2.0		0.5				23.4
	7	34.0		17.0	26.5	0.5	0.5					0.5			0.5		0.5	20.0
	24	37.5		47.5	10.0							2.0				0.5	1.0	1.5
MC2	35	54.2		37.8	1.5		0.5					1.5		0.5		0.5		3.5
	50	41.6		36.6	5.4	2.0						5.0	1.0			2.5		5.9
	80	43.2		42.7	7.8	1.0						1.9		2.9				0.5
	100	55.4	0.5	27.2	7.4	1.0			0.5			2.5		1.0				4.5
	10	5.0				94.0												1.0
	18	23.3		4.5	0.5	67.2						1.0		1.0				2.5
	27	23.6		66.4	2.5	0.5					3.0	0.5		1.5				2.0
	40	10.9		80.6	5.0							1.0		0.5				2.0
MC3	47	45.3		22.2	13.8						0.5	4.4		1.5		1.0		11.3
	58	0.5		90.5	5.5							3.0				0.5		
	70	58.2		32.8	4.0							2.0		0.5				2.5
	80	51.3		12.2	3.0						16.5	1.7	0.9	5.7		1.3		7.4
	88	52.0		31.5	12.0		0.5					1.0						3.0

Table 2

Sample Name	Laboratory Sample code	Nature of sample	Radiocarbon Age (^{14}C yr BP)	AMS $\delta^{13}C$ (‰)	Calibrated Age Range (2 σ) (cal yr BP)
MC02	UB16441	Bivalve shell from hardground	6452 ± 32	1	6887 - 6567
MUS 17B	UB16449	Bone	Undetermined		
MUS 28/01/08	UB16450	Barnacle *Coronula diadema* from close to left scapula	5032 ± 30	-4.7	5304 - 4957
MUS 09 110.M	UB16451	Articulated bivalve *Barbatia* from material next to vertebrae	4743 ± 27	-1.5	4914 - 4574
MUS 11	UB16452	*Barbatia* shell from orange shelly layer banked against skull	5002 ± 29	-0.8	5285 - 4922

Note: Calibration utilised the CALIB (version 7.0.0) (Stuvier and Reimer, 1993) to 2 sigma employing a marine calibration curve and a regional reservoir age correction (ΔR) of 180 ± 53 derived from a sample of known age collected within the Persian Gulf to the east of Qatar (Hughen et al., 2004).

Table 3

Sample	Laboratory code	Depth (cm)	Palaeodose (De) (Gy)	Dose rate (µGy/a-1)	OSL age (ka BP)
MUS OSL 1a	Shfd11039	137	4.05 ± 0.23	1275 ± 63	3.18 ± 0.24
MUS OSL 2a	Shfd11040	98	2.47 ±0.08	884 ± 46	2.79 ± 0.17
MUS OSL 3a	Shfd11041	68	2.40 ± 0.07	955 ± 47	2.51 ± 0.14
Adjusted for potential dose-rate problems (see text for details)					
MUS OSL 1a	Shfd11039	137	4.05 ± 0.23	675 ± 32	6.00 ± 0.45
MUS OSL 2a	Shfd11040	98	2.47 ±0.08	365 ± 14	6.76 ± 0.34
MUS OSL 3a	Shfd11041	68	2.40 ± 0.07	452 ± 18	5.31 ± 0.27

Note: Ages are presented at 1 sigma confidence incorporating systematic uncertainties with the dosimetry data, uncertainties with palaeomoisture and errors associated with De determination.

Table 4

Sample name	Nature of sample	$\delta^{13}C$ (‰V-PDB)	$\delta^{18}O$ (‰V-PDB)	Calculated temperature (°C)
MUS09 110.M	Articulated bivalve *Barbatia* from next to whale	1.65	2.34	22.6
MUS09 148.M	Articulated bivalve *Pinctada* from next to whale	1.37	1.16	27.7
MUS09 183.M	Articulated bivalve *Pinctada* from next to whale	2.22	0.51	30.5

Table 5

Location	Transgression past present sea level	Highstand	Regression to present sea level	Maximum sea level (+m)	Author
Indian Ocean					
Malay-Thai Peninsula		4850-4450 cal yr BP		5	Horton et al., 2005
Mozambique	6500 BP	4480 BP	900 BP	2.75	Ramsay, 1995
Maldives	4500 cal yr BP	4000-2100 cal yr BP		>0.5 ±1	Kench et al., 2009
Sri Lanka		4900-4000 BP	3000 BP		Ranasinghe et al., 2013
SE Asia					
Papua New Guinea		5800 ^{14}C yrs BP			Chappell and Polach, 1991
Strait of Malacca		4980 ^{14}C yrs BP		5	Geyh et al., 1979
Cocos Islands		after 3000 ^{14}C yrs BP		>0.5	Woodroffe and McLean, 1990
Phuket, Thailand		6000 BP		1	Scoffin and Le Tissier, 1998
S. China		5140 ±50 yr BP		<2	Yim and Huang, 2002
Thai-Malay Peninsula	6 ka	5 ka	1.5 ka (Thailand)	5	Tjia, 1996
Vietnam		6.7-5 ka		1.4-1.6	Stattegger et al., 2013
Australia					
W Australia		5660 ±50-4040 ±50 ^{14}C yrs BP		1.65	Beaman et al., 1994
E Australia		3420-1780 BP		>1	Flood and Frankel, 1989
E Australia		4150-3470 BP		1.7	Baker and Haworth, 2000
S Australia		5100 BP		2.2	Baker et al., 2000
SW Australia		7 ka		2	Collins et al., 2006
Pacific					
Central Equatorial Pacific		5000-1500 BP		1-2	Grossman et al., 1998
Fiji Islands	before 6900 ^{14}C yrs BP	5650-3200 ^{14}C yrs BP		1.35-1.5	Nunn and Peltier, 2001
Atlantic					
S Carolina, USA		4.2 ka			Gayes et al., 1992
Florida, USA	7.5 ka				Van Soelen et al., 2010
South Africa		6.8 ka	4.9 ka	0-3	Compton, 2001
Brazil	7550-6500 cal yr BP	5800-2000 cal yr BP		2-3	Angulo et al., 2006
Bahamas		3000 BP		1.5	Bourrouilh-Le Jan, 2007

Figure 1
Click here to download high resolution image

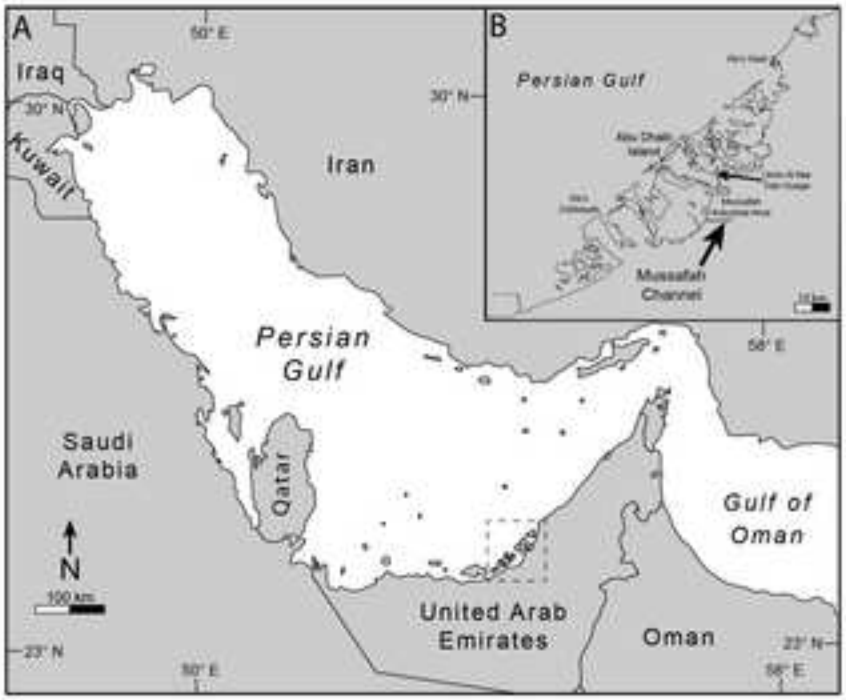

Figure 2

Click here to download high resolution image

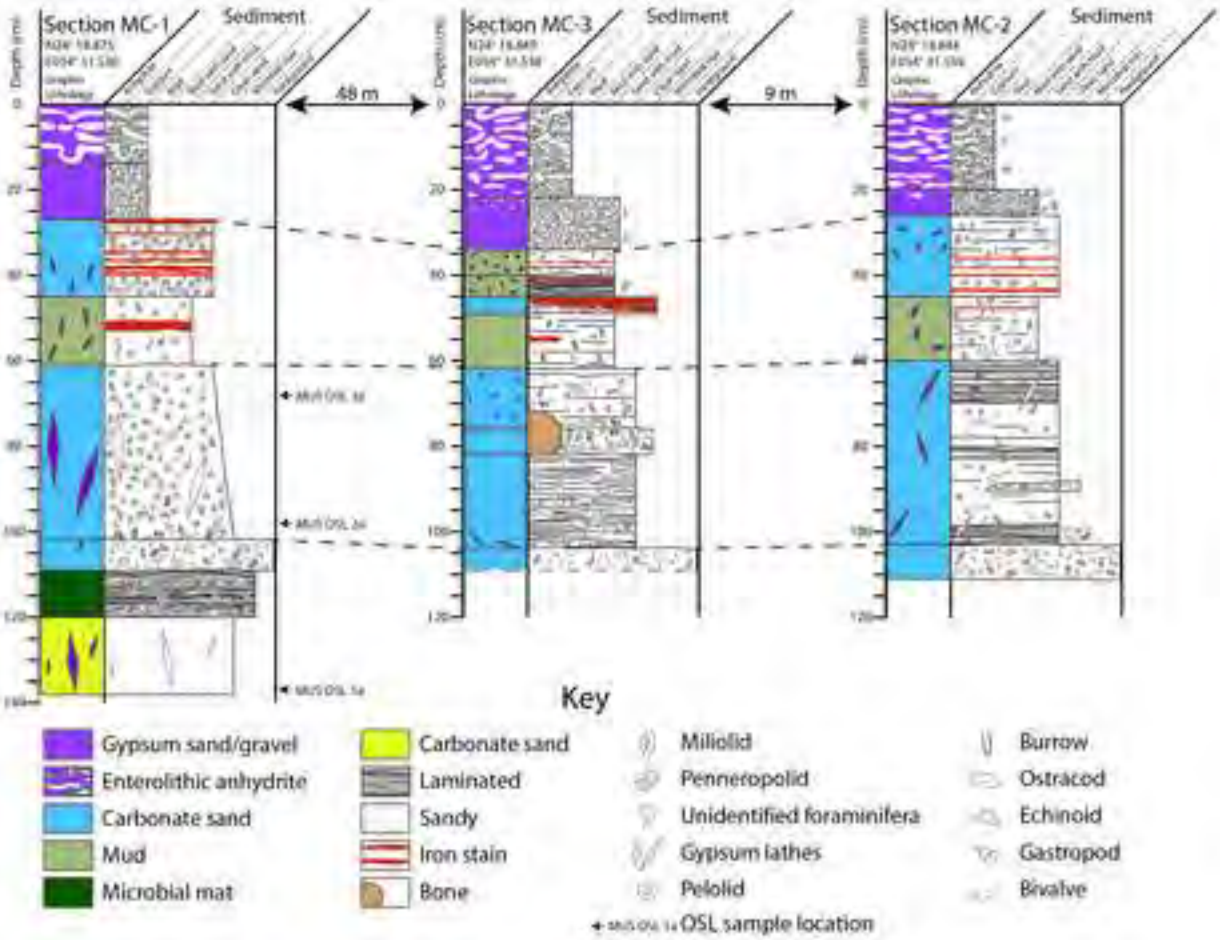

Figure 3

Click here to download high resolution image

Figure 4
Click here to download high resolution image

Figure 5

Click here to download high resolution image

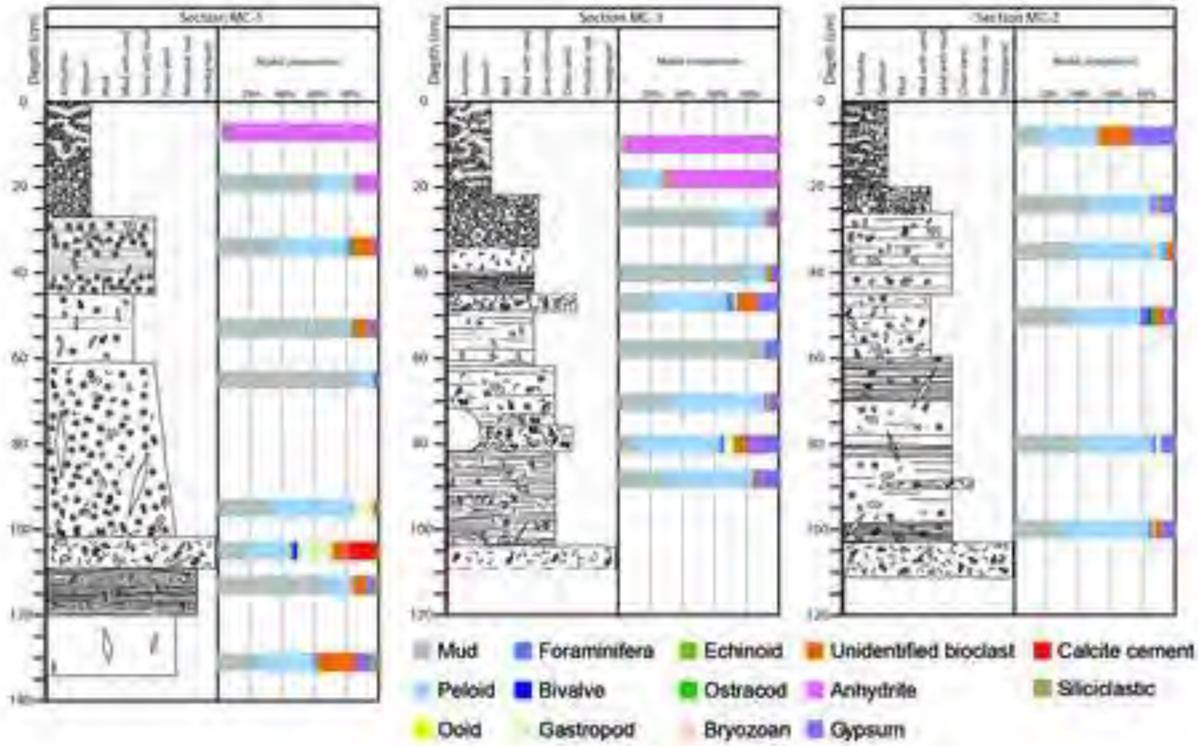

Figure 6

Click here to download high resolution image